

Production and measurement of $e^+e^- \rightarrow c\bar{c}$ signatures at the 250 GeV ILC

A. Irles^{1a,b}, R. Pöschl^{a,b}, F. Richard^{a,b}

^aon behalf of the ILD concept group

^bUniversité Paris-Saclay, CNRS/IN2P3, IJCLab, 91405 Orsay, France

Abstract

This document discusses for the first time the experimental prospects on the measurement of cross section and the forward-backward asymmetry in $e^+e^- \rightarrow c\bar{c}$ collisions at 250 GeV at the International Linear Collider operating polarised beams. The cross section will be normalised to the total hadronic cross section. We discuss the results for an analysis assuming the integrated luminosity of 2000 fb⁻¹ foreseen in the baseline project. The measurement requires determining the charge of both jets identified as originated by a c -quark. The charge measurement is optimally performed using the precise micro-vertex detector of the detector ILD and the charged kaon identification provided by the dE/dx information of its TPC. Thanks to the beam polarisation, we can separate the four independent chirality combinations of the electroweak couplings, enhancing in this way the sensitivity to new physics effects. We show that due to the unprecedented precision that will be achieved by the ILC for these observables, the ILC will be sensitive to the existence of beyond the standard model Randal Sundrum resonances of several tens of TeV.

1. Introduction

The c -quark (and b -quark) electroweak couplings to the Z -boson have been determined [1] by the LEP1 detector collaborations and the SLD Collaboration in $e^+e^- \rightarrow c\bar{c}$ (and $e^+e^- \rightarrow b\bar{b}$) collisions at the Z -pole. These couplings are usually determined from the measurement of experimental distributions such as the $e^+e^- \rightarrow c\bar{c}$ (and $e^+e^- \rightarrow b\bar{b}$) cross section divided by the total hadronic cross section and the forward-backward asymmetry. The measurements done by LEP1 detector collaborations profited from higher luminosities recorded than the SLD ($\sim \times 20$ times more). Despite the large difference on integrated recorded luminosity, the SLD obtained a similar precision measurements due to the benefits of having a polarised beam and a smaller radius of the vacuum beam pipe that permitted instrumenting the tracker closer to the interaction point.

The cross section normalised to the total hadronic cross section is defined as:

$$R_q = \frac{\sigma^{q\bar{q}}}{\sigma^{had.}} \quad (1)$$

where $\sigma^{q\bar{q}}$ is the $e^+e^- \rightarrow q\bar{q}$ total cross section for given q -quark flavour and $\sigma^{had.}$ is the cross section for all q -quark flavours.

The forward-backward asymmetry is defined as:

$$A_{FB}^{q\bar{q}} = \frac{\sigma_F^{q\bar{q}} - \sigma_B^{q\bar{q}}}{\sigma_F^{q\bar{q}} + \sigma_B^{q\bar{q}}} \quad (2)$$

¹Corresponding author.

where $\sigma_{F,B}^{q\bar{q}}$ is the differential $e^+e^- \rightarrow q\bar{q}$ cross section integrated over the forward/backward hemisphere as defined by the polar scattering angle θ of the $\vec{p}_{b\bar{b}} = \vec{p}_b - \vec{p}_{\bar{b}}$. The z -axis of the right-handed coordinate frame is given by the direction of the incoming electron beam.

These two observables have been measured at the Z -pole by the LEP experiments and by the SLD. At the Z -pole, the R_q observable is interpreted as $R_q = \frac{\Gamma_{q\bar{q}}}{\Gamma_{had.}}$ where $\Gamma_{q\bar{q}}$ is the decay width of $Z \rightarrow q\bar{q}$ and $\Gamma_{had.}$ is the total hadronic Z -decay width. The R_c and $A_{FB}^{c\bar{c}}$ observables were measured with experimental precisions of 2% and 4% respectively.

The International Linear Collider (ILC) [2, 3, 4, 5, 6] is a linear electron-positron collider with polarised beams that will produce collisions at several energies. In this document, we discuss the prospects for the measurements of these two observables at the ILC operating at a centre of mass energy of 250 GeV (ILC250). At energies far above the Z -pole the experimental observables are sensitive to the interference between the γ the Z and potential new vector bosons.

The International Large Detector (ILD) [6] is one of the proposed detectors to measure the interactions. This detector will be optimised to use Particle Flow (PF) reconstruction algorithms [7, 8, 9] in order to reconstruct and separate individual particles produced in the collisions. For this, a high granularity calorimetric system is foreseen to be placed inside a ~ 4 T magnetic field. Moreover, the ILD will have a high precision tracking system with the first layer placed at 16 mm from the interaction point to maximise the tracking and vertex reconstruction capabilities. The central tracker of the ILD is a Time Projection Chamber (TPC) that provides pattern recognition with more than 200 space points.

2. Event reconstruction and selection

All results shown here are obtained using detailed simulation of the ILD concept [6]. The experimental studies are made for the case in which the electron and positron beams are 100% polarised. We use the following notation: $e_L p_R$ for the cases in which the electron beam has 100% left polarisation and the positron beam has 100% right polarisation (and vice versa for $e_R p_L$). The size of the analysed samples is the equivalent of 250 fb $^{-1}$ for each of the processes while the ILC250 programme foresees a total of 2000 fb $^{-1}$ shared between the different beam polarisations schemes: 900 fb $^{-1}$ for each of the $P(e^-, e^+) = (\pm 80\%, \mp 30\%)$ and 100 fb $^{-1}$ for $P(e^-, e^+) = (\pm 80\%, \pm 30\%)$. Final results will be scaled to the foreseen luminosity.

The events are generated at leading order using the WHIZARD 1.95 [10, 11] event generator. The parton showering and hadronisation are simulated by the Pythia 6.422 event generator [12]. The ILD detector geometry and the interaction of the particles with the detector are simulated within the Mokka framework interfaced with the Geant4 toolkit [13, 14, 15]. The different reconstruction algorithms are implemented in the ILCSoft toolkit. We make use of the tracking, quark-tagging, particle identification in the TPC and jet clustering algorithms described in Ref.[16]. The primary and secondary vertex reconstruction has special importance for this analysis. Therefore they were optimised to fit the high precision requirements of this analysis (see, again, Ref. [16] for more details).

The $e^+e^- \rightarrow q\bar{q}$ events have a very distinguishable signature, in which both quarks are observed as a two jet back-to-back system at same energy. Events are reconstructed using the Durham jet algorithm forced to form two jets. Leptonic events are removed by a selection of two hadronic jets. Backgrounds are given by: the events that are subject to a radiative return to the Z -pole due to initial state radiation and di-boson events with hadronic decays. These backgrounds are rejected by a combination of three cuts:

1. A cut on the y_{23} distance that defines the Durham distance at which a two jet system would be reconstructed as a three jet system;
2. A cut on the sum of the two jet masses. This cut helps reducing the impact of QCD final state radiation that dilutes the back-to-back configuration of the two jets and also helps suppressing the background from $WW/ZH/ZZ$ events.

3. A cut on the sphericity of the event. This cut depends on the polar angle at which the jets are reconstructed since by ISR the system receives a boost, *i.e.* is not back-to-back anymore and/or receives a transverse momentum.

The values of these cuts can be found in the legend of the Figure 1, left. A more detailed discussion on the selection procedure can be found at the Appendix 6. With these cuts, we select a clean sample of $e^+e^- \rightarrow q\bar{q}$ with $q = u, d, s, c, b$. The efficiency of selection is shown as a function of the $\cos\theta_q$ angle absolute value. The selection efficiency is slightly different between the light and heavy quarks. These differences come from the quark mass differences: the larger the quark mass, the harder and less collinear the gluon final state radiation [17, 18] and are well explained by QCD.

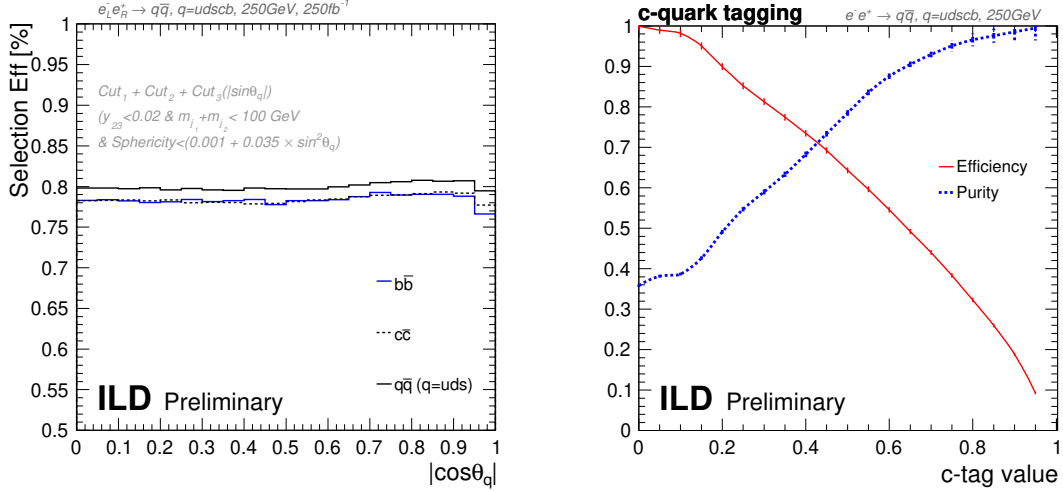


Figure 1: Left plot: efficiency of the preselection for the different quark flavours vs the angular distribution of the two jet system. Right plot: efficiency and purity of the c -quark tagging.

For the final step of our pre-selection of $e^+e^- \rightarrow c\bar{c}$, we suppress the most dominant background, the $e^+e^- \rightarrow q\bar{q}$ ($q = u, d, s, b$), by requiring that one or two jets have a large c -tag value ($c\text{-tag} > 0.875$). The quality, in terms of efficiency and purity, of the c -quark tagging for 125 GeV jets as a function of the c -tag value is shown in the right plot from Figure 1.

The impact of all the selection cuts on the signal selection efficiency and the ratio of background vs signal is summarised in Table 1 and in Figure 2.

3. R_c measurement

To reach the maximum of precision on the measurement of R_c , we will measure it at the same time as we measure the c -quark tagging efficiency applying the Double Tag approach described in [1]. The method is as follows: first we count the fraction of jets in the preselected events that are tagged as a c -jet. This ratio is denominated f_1 . To use this method we have to assume that we know the value of R_b , ϵ_b and ϵ_{uds} or that we measure them at the same time. This measurement will also depend on the other sources of backgrounds which are very much reduced by the preselection and that are expected to be known to the percent level or better, so they can be ignored at the first approach. Secondly, we measure the fraction of preselected events in which both jets have been tagged as c -jets. This quantity is f_2 and has similar dependencies as f_1 with the addition of the correlation variable ρ_c . This correlation factor accounts for the correlations due to displacements of primary vertex determination (common for both jets), purely geometric correlations associated to differences between the detector

$eLPR$							
	Signal [%]	Background processes [%] (B/S [%])					
	$c\bar{c}$	$b\bar{b}$	$q\bar{q} (uds)$	$\gamma q\bar{q}$	ZZ	WW	HZ
Cut_1	85.6	85,2 (69,1)	87,2 (224,0)	69,0 (53,2)	15,4 (3,1)	16,7 (35,1)	11,0 (0,2)
$Cut_1 + Cut_2$	82,1	82,1 (69,4)	83,7 (224,4)	65,7 (52,8)	8,2 (1,7)	10,5 (23,1)	5,3 (0,1)
$Cut_1 + Cut_2 + Cut_3$	78.5	78,4 (69,4)	80,0 (224,4)	24,5 (20,6)	4,1 (0,9)	3,2 (7,4)	2,3 (0,0)
$Cut_1 + Cut_2 + Cut_3 + 1ctag$	38.9	2,1 (3,8)	0,2 (0,9)	1,1 (1,9)	0,3 (0,1)	0,2 (0,8)	0,1 (0,0)
$Cut_1 + Cut_2 + Cut_3 + 2ctag$	7.3	0,0 (0,2)	0,0 (0,0)	0,1 (0,7)	0,0 (0,0)	0,0 (0,1)	0,0 (0,0)

$eRPL$							
	Signal [%]	Background processes [%] (B/S [%])					
	$c\bar{c}$	$b\bar{b}$	$q\bar{q} (uds)$	$\gamma q\bar{q}$	ZZ	WW	HZ
Cut_1	85.6	85,1 (35,8)	87,1 (161,4)	69,0 (38,8)	17,7 (3,6)	7,8 (0,4)	10,9 (0,4)
$Cut_1 + Cut_2$	82.2	82,0 (36,0)	83,7 (161,5)	65,7 (38,5)	10,7 (2,3)	4,7 (0,2)	5,3 (0,2)
$Cut_1 + Cut_2 + Cut_3$	78.6	78,2 (35,9)	80,0 (161,5)	24,4 (15,0)	5,5 (1,2)	1,4 (0,1)	2,3 (0,1)
$Cut_1 + Cut_2 + Cut_3 + 1ctag$	38.9	2,1 (2,0)	0,2 (0,6)	1,3 (1,6)	0,4 (0,2)	0,2 (0,0)	0,1 (0,0)
$Cut_1 + Cut_2 + Cut_3 + 2ctag$	7.3	0,0 (0,1)	0,0 (0,0)	0,1 (0,7)	0,0 (0,1)	0,0 (0,0)	0,0 (0,0)

Table 1: Percentage of the signal and the different background events remaining after each selection step. For completeness, the background to signal ratio (in % units) is also quoted. It is important to remark that the efficiencies shown for $\gamma q\bar{q}$ are calculated for a sample which has already a cut at the generation level to remove most of the radiative return events. All these events are removed with the first two cuts.

inhomogeneities and QCD related effects associated to hard gluon emission. The two ratios and their dependence on the different terms are described in the following equations:

$$\begin{aligned}
f_1 &= \epsilon_c R_c + \epsilon_b R_b + \epsilon_{uds}(1 - R_c - R_b) + F(\epsilon_c, \epsilon_b, \epsilon_{uds}, BKG) \\
f_2 &= \epsilon_c^2(1 + \rho_c)R_c + \epsilon_b^2 R_b + \epsilon_{uds}^2(1 - R_c - R_b) + F(\epsilon_c^2, \epsilon_b^2, \epsilon_{uds}^2, BKG)
\end{aligned} \tag{3}$$

In this method, the statistical uncertainty is determined by the size of the double tagged sample, which is proportional to the square of the tagging efficiency. In the past, only the SLD Collaboration was able to present a high precision R_c measurement using the Double Tag technique [19], thanks to a superior c -quark tagging. For the ILD case, the ϵ_c is of the order of the 35% which is almost twice what the SLD achieved [19].

The reconstructed f_1 and f_2 distributions are shown in the second and third rows of Figure 2. The angular distribution of the estimated ϵ_c and ρ_c can be seen in Figure 3 (red graphs).

3.1. Experimental systematic uncertainties

The tagging efficiency ϵ_c is the main source of uncertainty on the determination of R_c , and we find that it can be determined at the per mille level. The other systematic uncertainties considered are close to negligible.

Correlation factor

The correlation factor is compatible with zero for most values of $\cos \theta$ and therefore it will not affect to the measurement of R_c and ϵ_c . It is important to remark that for the measurements made at LEP1 and SLD, this factor was of the order of the few percent and had a significant impact on the systematic uncertainty not only for the c -quark case, but also for the b -quark case. Due to the small size of the beam spot expected at the ILC and the proximity to the beam line of the first tracking layers in the ILD, the correlation effects will be very much reduced.

For 250 GeV collisions, R_b is more or less a factor two lower than R_c and it will be measured at the per mille level [20], when recorded 2000 fb⁻¹ of luminosity.

Tagging and mistagging efficiencies

The high purity of the c -tagging of ILD corresponds to small values of ϵ_b of 1.3%. Using control samples (for example, considering only events in which one jet is tagged as a b -quark jet with high purity) this value could be measured to better than 1%, assuming a factor two improvement from [19]. For the lighter quarks, ϵ_{uds} , is almost negligible $\epsilon_{uds} = 0.1\%$ and has a minimal impact on the extraction of ϵ_c and R_c . It can be extracted from MC: current knowledge of the $g \rightarrow c\bar{c}$ coupling is

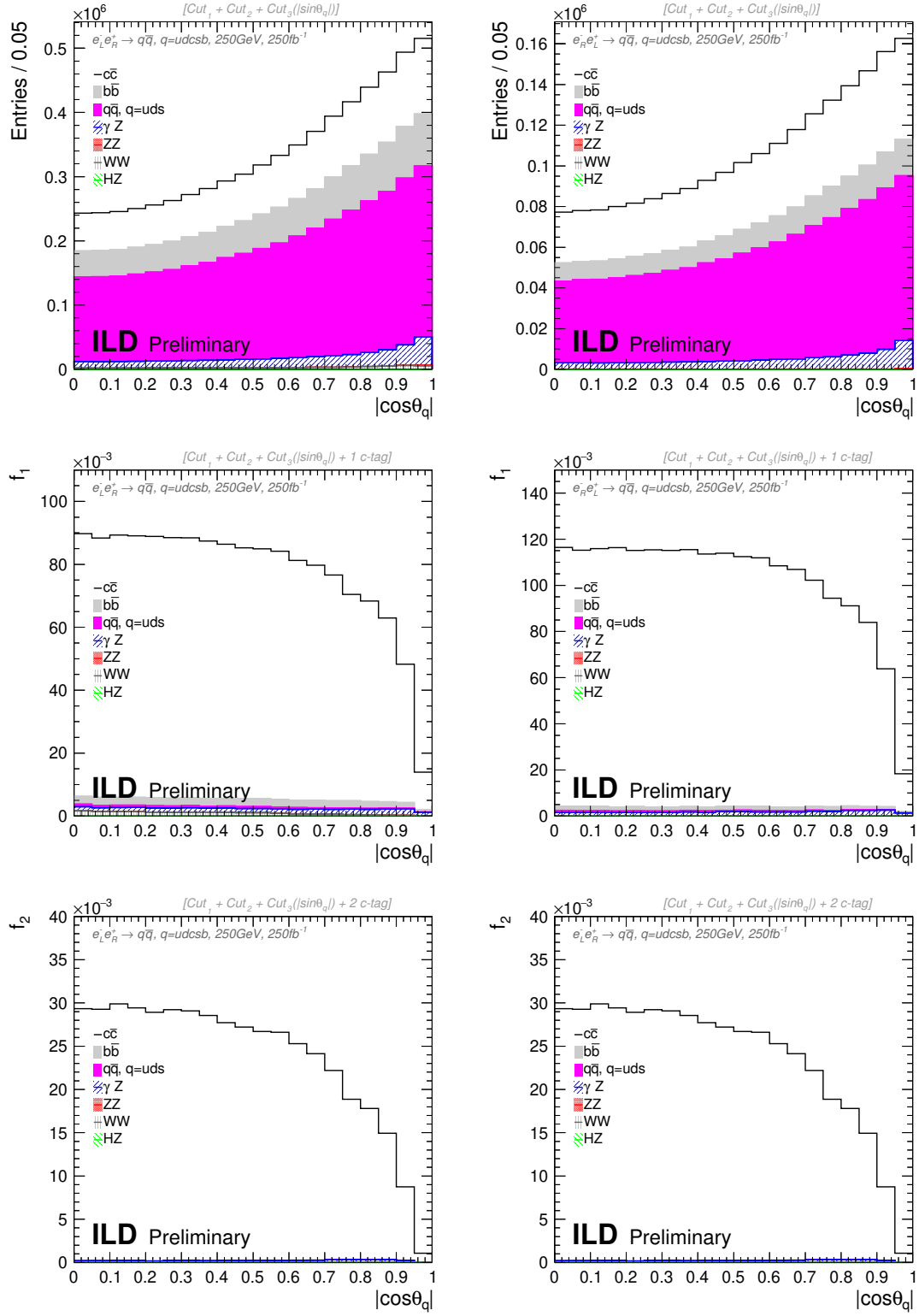


Figure 2: First row: distribution of preselected 2-jet distributions. Second row: the f_1 distribution as defined in Eq. 3. Third row: the f_2 distribution as defined in Eq. 3. All distributions are shown for the 100% left and right handed polarisation cases.

known to 12%[1]. The value of both mistagging efficiencies ϵ_b and ϵ_{uds} should also account for the small differences observed in the preselection between flavours, due to the quark mass effects. These differences are of the order of the 1-2% and are estimated to be known to 1-10% [17, 18]. Therefore this effect will affect minimally the determination of the different ϵ_c .

Background subtraction

In contrast with previous experiments where the collisions occurred at the Z -mass resonance dominating the signal, we will have other background contributions to the preselection that will be of the order of the 20% of the total $c\bar{c}$ signal. The dominating one will be the radiative return. We expect to understand this background to better than 1% level from $e^+e^- \rightarrow Z \rightarrow q\bar{q}$ measurements during the GigaZ physics program of the ILC [21, 22]. Therefore, this effect will also have minimal impact on the determination of the different ϵ_q .

Beam polarisation

For the estimation of the uncertainties due to the measurement of the beam polarisation, we take the numbers from [23].

Beam polarisation uncertainty			
ΔP_{e-}^- [%]	ΔP_{e-}^+ [%]	ΔP_{e+}^- [%]	ΔP_{e+}^+ [%]
0.1	0.04	0.1	0.14

Table 2: Uncertainty on the beam polarisation. Numbers extracted from [23]

Since the total cross section depends on the polarisation of the beams, it will affect the final result. However, due to the reduced beam polarisation uncertainties and that the observable is a ratio, the impact is negligible.

3.2. Results

After all these considerations, we estimate that the ϵ_c will be determined with a precision of at least 0.2% for a recorded luminosity of 2000 fb⁻¹. This is translated to the following expectations for the precision on R_c for the two beam polarisations for the ILC250 physics programme:

$$\begin{aligned}\Delta R_c(e_L p_R) &= 0.10\%(stat.) + 0.16\%(syst.) \\ \Delta R_c(e_R p_L) &= 0.13\%(stat.) + 0.17\%(syst.)\end{aligned}\tag{4}$$

for a total luminosity of 2000 fb⁻¹.

4. Measurement of $A_{FB}^{c\bar{c}}$

After the selection of a highly pure $c\bar{c}$ sample, we need to determine the jet charges to reconstruct the angular distribution. The c -quarks mostly produce $D^0/D^\pm/D_s$ -mesons. The decay branching ratio of D^0 to charged kaons is $\sim 50\%$. For the D_s this number is somewhat lower: $\sim 33\%$. The D^\pm produce one and three prongs in their decays, with only $\sim 30\%$ of the cases having a charged kaon in the final state. In all cases, identifying a kaon in a secondary vertex gives direct information on the charge of the original c -quark. This method of quark charge determination is called *Kaon-method*. If the Kaon is not identified, the total charge of the reconstructed secondary vertex is used. This is specially interesting for the decays involving D^\pm -mesons. This second method is called *Vtx-method*. To apply these methods, we require excellent tracking, vertexing and particle identification capabilities. While ILD has a 99% probability to reconstruct the relevant charged tracks, this probability falls to 96% for tracks connected to the micro-vertex and having a significant offset. Revisiting the tracking and vertexing algorithms to improve this value is an ongoing activity in the collaboration. This probability

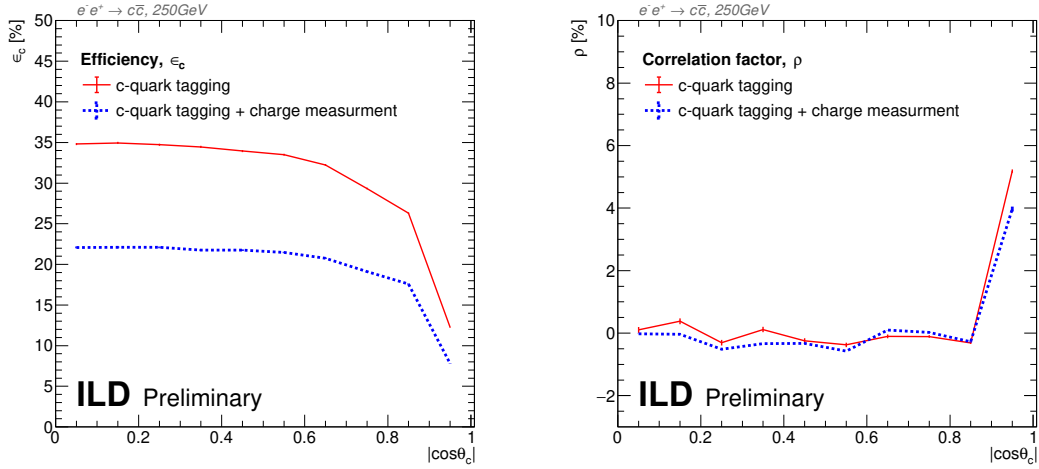


Figure 3: Efficiency (left) and correlation factor (right) for c -quark tagging and c -quark charge measurement.

drops rapidly for jets reconstructed at $|\cos \theta| > 0.9$ due to imprecise track reconstruction outside of the acceptance of the micro-vertex detector. Modifying this geometry and/or prolonging the first layer of the barrel is under consideration by the collaboration. Due to the high granularity of the ILD TPC, the power of separation of kaons and other hadrons is large enough to provide kaon identification with high efficiency and purity for jets with $|\cos \theta| < 0.9$ and momentum above 3 GeV. For this process, kaons are identified with a purity reaching 90% at 88% efficiency.

The charge measurement allows us to attribute a sign to the reconstructed $\cos \theta_c$ value. However a sign-flip may be induced due the missed tracks in a reconstructed vertex and the misidentification of kaons. In order to correct for that, we need to know with high precision the probability of getting the charge correctly using the different methods. This probability is called purity and it is measured using the data itself by comparing two different reconstructed samples in which the charge of both jets has been measured: the sample in which both jets were estimated to have different/the same charge. The method is described in detail in [20]. The purity of each method is shown in the left plot of Figure 4. Once that the purity of each method is well known, we can apply it to correct the charge mismeasurements on the reconstructed distributions. The performance of the method is shown in the left plot of Figure 4.

The final reconstruction efficiency requiring at least one jet with the charge measured is of the 25.7% (20.8% using the *Kaon*-method and using the 5.9% *Vtx*-method). The determination of the $A_{FB}^{c\bar{c}}$ value is done by integrating the measured distribution. This distribution is shown in Figure 5 (upper row) for both polarisations. For completeness, we also show the distributions with double charge measurement. This is done after the correction of the charge migrations and after the selection efficiency corrections are applied. The latter is done by measuring the c -tagging plus charge calculation efficiency, $\epsilon_{c,charge}$, in the same way as in the R_c case, but applying c -tagging and charge measurement at the same time.

4.1. Experimental systematic uncertainties

The measurement of $A_{FB}^{c\bar{c}}$ mostly suffers from the same systematic uncertainties as R_c . Therefore we will only describe the points that are specific for this observable.

The expected $\epsilon_{c,charge}$ and the corresponding correlation factor are shown in Figure 3 as blue dotted lines and will be determined with a precision of the order of 0.3%. It is important to remark that as the $A_{FB}^{c\bar{c}}$ is a ratio in which the tagging efficiency will appear in both the numerator and denominator. For

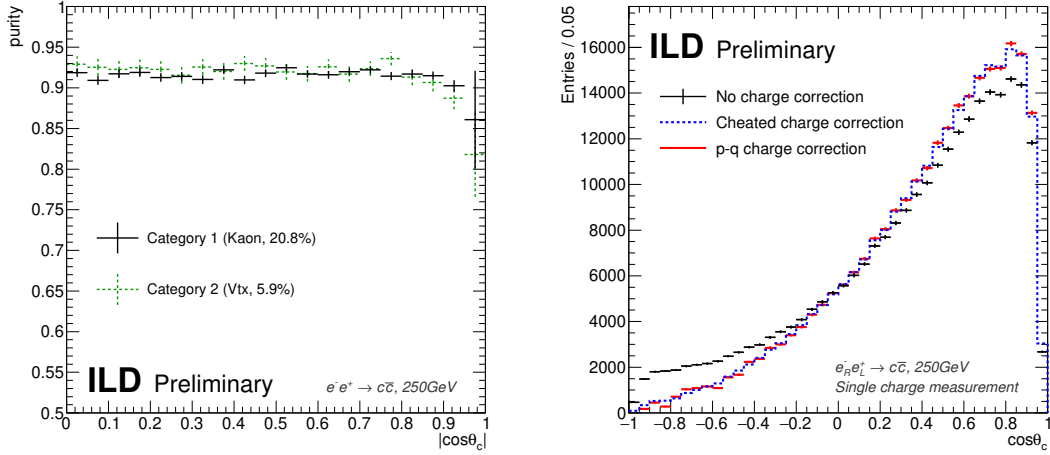


Figure 4: Left plot: Measured purity of each method. Right plot: the performance of the p-q in single events: p-q is calculated using double tagged events but it is applied to single charge events.

R_c , the tagging efficiency (and mistagging efficiencies) appeared only in the numerator. Therefore, we are not interested in the global value of $\epsilon_{c,charge}$ but in the relative variations between the correction factors. In any case, for safety, we will reduce the analysis of the distribution to values of $|\cos\theta| < 0.75$ before the drop in $\epsilon_{c,charge}$. There is a second effect that is also corrected for: the inhomogeneities on the preselection efficiency as a function of $|\cos\theta|$. This is seen in the left plot of Figure 1 where small differences of the $\sim 1\%$ are observed. Due to the reduced size of such inhomogeneities, their impact will be minor and will not affect the final result if they are known at the level of a few percent which will be achievable with controlled samples or with simulations.

4.2. Results

The final distributions for both polarisations fitted to the leading-order estimation are shown in Figure 6.

The expected precision on the forward-backward asymmetry measurements are, for a recorded luminosity of 2000 fb^{-1} :

$$\begin{aligned}\Delta A_{FB}^{c\bar{c}}(e_L p_R) &= 0.16\%(stat.) + 0.09\%(syst.) \\ \Delta A_{FB}^{c\bar{c}}(e_R p_L) &= 0.20\%(stat.) + 0.10\%(syst.)\end{aligned}\tag{5}$$

5. Prospects for BSM discoveries

The results on the expected experimental precisions foreseen for ILC running at 250 GeV are summarised in the previous sections. For both observables, and both polarisations, total experimental uncertainties of $\sim 0.2\%$ are expected for the full 2000 fb^{-1} program. Such accuracies consist a challenge to theoretical high order corrections, particularly for what concerns the electroweak corrections. It is out of the scope of this document to discuss this issue.

Many beyond standard models with extended gauge structures [24, 25, 26] predict large corrections for the standard model electroweak couplings. Therefore, these models predict large modifications of the forward backward asymmetry and the cross section. Some of these models, for example [25], predict that such kind of effects for all fermions (not only for the heaviest). The unprecedented precision that will be achieved at the ILC allows to deeply investigate all these models. Of particular

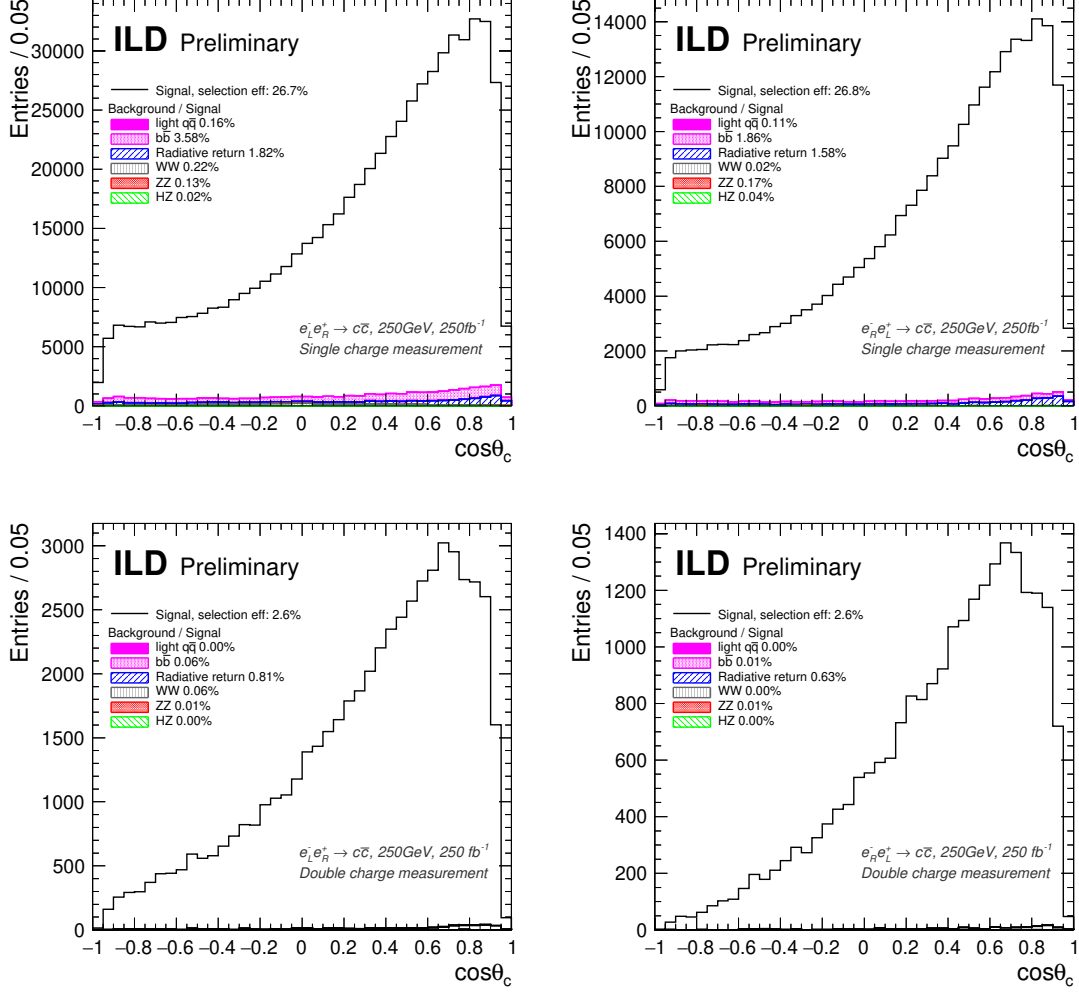


Figure 5: Differential signal and background distributions after the charge calculation using the Vtx - and $Kaon$ -method defined above. We compare distributions in which both jets have compatible charges (lower row) or in which only one jet with charge is required (upper row).

importance is the fact that - thanks to the beam polarisation at the ILC - we could inspect the different helicity amplitudes in order to disentangle between the different models. The expected precision on the determination of the helicity amplitudes can be compared with the SM and any BSM predictions. This is done in Figure 7 for several models, extracting the helicity amplitudes from the R_c , $A_{FB}^{c\bar{c}}$ and R_b , $A_{FB}^{b\bar{b}}$ [20]. It shows that a modest energy of 250 GeV, the ILC has a reach which extends well above LHC direct searches. For what concerns the Hosotani model [25], the large effect seen for a 8 TeV resonance indicates that ILC250 can extend its sensitivity even far beyond. In the absence of a signal, one would conclude that such a Z' is heavier than 34 TeV at 95% C.L.

6. Summary

This document summarises the results of a realistic analysis based on full detector simulation and reconstruction of $e^+e^- \rightarrow c\bar{c}$ processes at the ILC. The results show a large improvement on the reachable

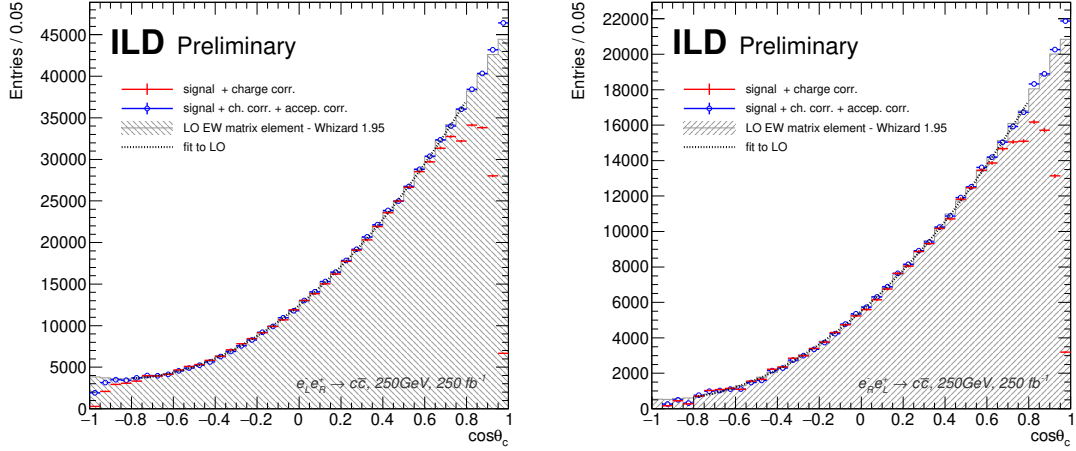


Figure 6: Reconstructed angular distribution for both polarisations. The red empty dots shows the reconstructed distribution before the efficiency and acceptance correction. The blue circles shows the corrected distribution. The shaded grey are shows the prediction at leading order (LO) and the grey curve shows the result of the fit of the LO to the final distribution in a constrained range of $\cos \theta_c$.

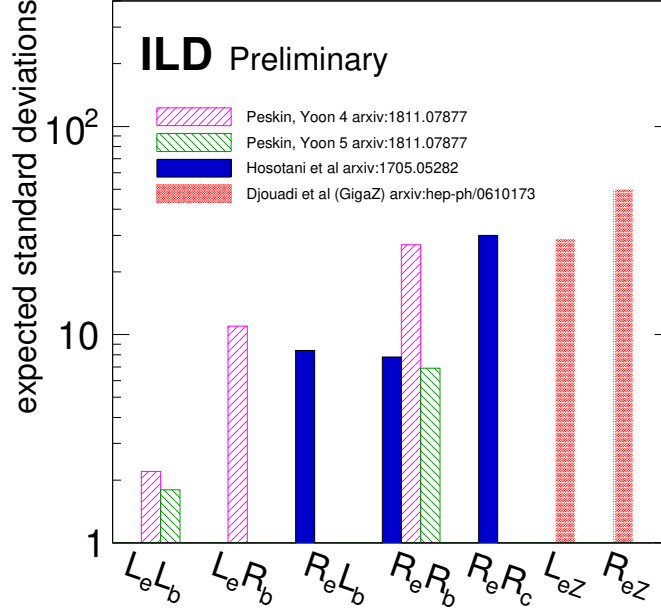


Figure 7: Expected number of standard deviations for different BSM scenarios when determining the different EW couplings to c - and b -quark at ILC250. The x -axis shows the different couplings for different chiralities, following the notation from [20]. The expectations for different BSM scenarios are shown: 1) for Djouadi [24] one assumes $m_{Z'} = 3$ TeV; 2) for the Peskin *et al.* model [26], two versions are given, labelled as Peskin 4 and Peskin 5; 3) for Hosotani et al. [25] one assumes $m_{Z'} \sim 8$ TeV for the 3 resonances. These prospects assume the input from the ILC GigaZ programme running at the Z -Pole [22] in order to improve by a factor ~ 5 the current precision on the SM Z -boson couplings to the different quarks measured at the Z -pole.

precisions compared with previous experiments. The measurement requires determining the charge of both jets identified as originated by a c -quark. This is possible thanks to expected exceptional vertexing capabilities of the ILD and the charged kaon identification provided by the dE/dx information of its high granularity TPC. Also highlighted is a major advantage compared with other experiments: the power of separation and the independent determination of the left and right handed components of the electroweak couplings thanks to the beam polarisation.

Acknowledgements

We would like to thank the LCC generator working group and the ILD software working group for providing the simulation and reconstruction tools and producing the Monte Carlo samples used in this study. This work has benefited from computing services provided by the ILC Virtual Organisation, supported by the national resource providers of the EGI Federation and the Open Science GRID.

References

References

- [1] ALEPH, DELPHI, L3, OPAL, SLD, LEP ELECTROWEAK WORKING GROUP, SLD ELECTROWEAK GROUP, SLD HEAVY FLAVOUR GROUP collaboration, S. Schael et al., *Precision electroweak measurements on the Z resonance*, *Phys. Rept.* **427** (2006) 257–454, [[hep-ex/0509008](#)].
- [2] T. Behnke, J. E. Brau, B. Foster, J. Fuster, M. Harrison, J. M. Paterson et al., *The International Linear Collider Technical Design Report - Volume 1: Executive Summary.* , [1306.6327](#).
- [3] H. Baer, T. Barklow, K. Fujii, Y. Gao, A. Hoang, S. Kanemura et al., *The International Linear Collider Technical Design Report - Volume 2: Physics.* , [1306.6352](#).
- [4] C. Adolphsen, M. Barone, B. Barish, K. Buesser, P. Burrows, J. Carwardine et al., *The International Linear Collider Technical Design Report - Volume 3.I: Accelerator & in the Technical Design Phase.* , [1306.6353](#).
- [5] C. Adolphsen, M. Barone, B. Barish, K. Buesser, P. Burrows, J. Carwardine et al., *The International Linear Collider Technical Design Report - Volume 3.II: Accelerator Baseline Design.* , [1306.6328](#).
- [6] H. Abramowicz et al., *The International Linear Collider Technical Design Report - Volume 4: Detectors*, [1306.6329](#).
- [7] J.-C. Brient and H. Videau, *The Calorimetry at the future e^+e^- linear collider*, *eConf C010630* (2001) E3047, [[hep-ex/0202004](#)].
- [8] V. Morgunov and A. Raspereza, *Novel 3-D clustering algorithm and two particle separation with tile HCAL*, [physics/0412108](#).
- [9] Sefkow, F. and White, A. and Kawagoe, K. and Pöschl, R. and Repond, J., *Experimental Tests of Particle Flow Calorimetry*, *Rev. Mod. Phys.* **88** (2016) 015003, [[1507.05893](#)].
- [10] W. Kilian, T. Ohl and J. Reuter, *WHIZARD: Simulating Multi-Particle Processes at LHC and ILC*, *Eur. Phys. J.* **C71** (2011) 1742, [[0708.4233](#)].
- [11] M. Moretti, T. Ohl and J. Reuter, *O’Mega: An Optimizing matrix element generator*, [hep-ph/0102195](#).

- [12] T. Sjöstrand, S. Mrenna and P. Skands, *PYTHIA 6.4 physics and manual*, *Journal of High Energy Physics* **2006** (may, 2006) 026–026.
- [13] GEANT4 collaboration, S. Agostinelli et al., *GEANT4: A Simulation toolkit*, *Nucl. Instrum. Meth. A* **506** (2003) 250–303.
- [14] J. Allison et al., *Geant4 developments and applications*, *IEEE Trans. Nucl. Sci.* **53** (2006) 270.
- [15] J. Allison et al., *Recent developments in Geant4*, *Nucl. Instrum. Meth. A* **835** (2016) 186–225.
- [16] S. Bilokin, *Hadronic showers in a highly granular silicon-tungsten calorimeter and production of bottom and top quarks at the ILC*. Theses, Paris Saclay, July, 2017.
- [17] DELPHI collaboration, P. Abreu et al., $m(b)$ at $M(Z)$, *Phys. Lett. B* **418** (1998) 430–442.
- [18] G. Rodrigo, A. Santamaria and M. Bilenky, *Do the quark masses run? extracting $m_b(m_Z)$ from cern lep data*, *Physical Review Letters - PHYS REV LETT* **79** (07, 1997) 193–196.
- [19] SLD collaboration, K. Abe et al., *Measurement of the branching ratio of the Z^0 into heavy quarks*, *Phys. Rev. D* **71** (2005) 112004, [[hep-ex/0503005](#)].
- [20] A. Irlles, R. Poeschl and F. Richard, *Determination of the electroweak couplings of the 3rd generation of quarks at the ilc*, *POS (EPS-HEP2019) 624* (to be published during 2020) .
- [21] K. Yokoya, K. Kubo and T. Okugi, *Operation of ILC250 at the Z-pole*, [1908.08212](#).
- [22] A. Irlles, R. Pöschl, F. Richard and H. Yamamoto, *Complementarity between ILC250 and ILC-GigaZ*, in *Linear Collider Community Meeting Lausanne, Switzerland, April 8-9, 2019*, 2019. [1905.00220](#).
- [23] R. Karl, *From the Machine-Detector Interface to Electroweak Precision Measurements at the ILC — Beam-Gas Background, Beam Polarization and Triple Gauge Couplings*. Dissertation, Universität Hamburg, Hamburg, 2019. 10.3204/PUBDB-2019-03013.
- [24] A. Djouadi, G. Moreau and F. Richard, *Resolving the $A(FB)^{**}b$ puzzle in an extra dimensional model with an extended gauge structure*, *Nucl. Phys. B* **773** (2007) 43–64, [[hep-ph/0610173](#)].
- [25] S. Funatsu, H. Hatanaka, Y. Hosotani and Y. Orikasa, *Distinct signals of the gauge-Higgs unification in e^+e^- collider experiments*, *Phys. Lett. B* **775** (2017) 297–302, [[1705.05282](#)].
- [26] J. Yoon and M. E. Peskin, *Fermion Pair Production in $SO(5) \times U(1)$ Gauge-Higgs Unification Models*, [1811.07877](#).

Appendix: Preselection

The event pre-selection proceeds as follows: we reconstruct events with two jets using the Durham algorithm. We could apply a cut in the invariant mass of the two jet system, in order to remove the most dominant background: radiative return to the Z -pole through ISR. However, this cut in the invariant mass would introduce a large difference on the preselection of the different quark flavours since the tails of the distribution highly depends on the quark flavour. This is mainly associated to the presence of neutrinos in the hadronisation and decay process, which is more common for heavy than light quarks. The invariant mass distribution of the two reconstructed jets can be seen in Figure 8.

To avoid the issue discussed above, we use topological variables instead of purely kinematic quantities. The first variable to be used is the Durham-distance y_{23} . The distribution of y_{23} for the different signals and backgrounds is shown in Figure 9, left plot. This variable corresponds to the jet clustering distance cut, as defined by the Durham algorithm, at which a two jet system would be reconstructed

as a three jet system. A cut of $y_2 < 0.02$ is applied. This cut introduces a residual flavour dependence due to the differences on QCD FSR due to the quark masses: the larger is the quark mass, the harder and less collinear is the QCD FSR therefore and therefore the higher is the possibility to have a 3-jet like event.

Further, a cut in the sum of the two jet masses is applied: if the sum of the two jet masses is greater than 100 GeV, the event is rejected. This cut helps reducing the impact of QCD final state radiation that dilutes the back-to-back configuration of the two jets and also helps suppressing the remaining background from ZZ events. See Figure 9 middle plot.

A last cut in the sphericity of the event follows. The sphericity tensor is defined as

$$S^{\alpha,\beta} = \frac{\sum_i p_i^\alpha p_i^\beta}{\sum_i |\vec{p}_i|^2} \quad \alpha, \beta = 1, 2, 3 \quad (6)$$

where p_i^α is the α -component of the momentum of the i -particle or jet. The eigenvalues of the sphericity tensor are called λ_1 , λ_2 and λ_3 (with $\lambda_1 \geq \lambda_2 \geq \lambda_3$ and $\lambda_1 + \lambda_2 + \lambda_3 = 1$). The sphericity is defined as $3/2(\lambda_2 + \lambda_3)$. Two jet like event have sphericity equal zero while completely isotropic events tend to have sphericity values equal to one. The sphericity distribution for the different signals and backgrounds is shown in Figure 9, last plot. The presence of ISR radiation has an impact in the sphericity of the event by unbalancing the momentum of the two jets. The ISR impact on the sphericity is dependent on the localisation of the event in the detector: two jets in the barrel in an event with ISR will have larger sphericity than an event with the same amount of ISR but with the two jets located in the forward/backward region. Therefore, applying a simple cut in the sphericity will give a difference on acceptance between the central and forward regions. We, therefore, apply a differential cut. The parametrisation of such cut is derived from Figure 10 (top left plot). The final efficiency as a function of $\cos\theta$ after the differential cut is shown in Figure 1. Similar cuts could be done using other related event shapes variables as the thrust or acolinearity. These options have been investigated and both perform similarly to the sphericity.

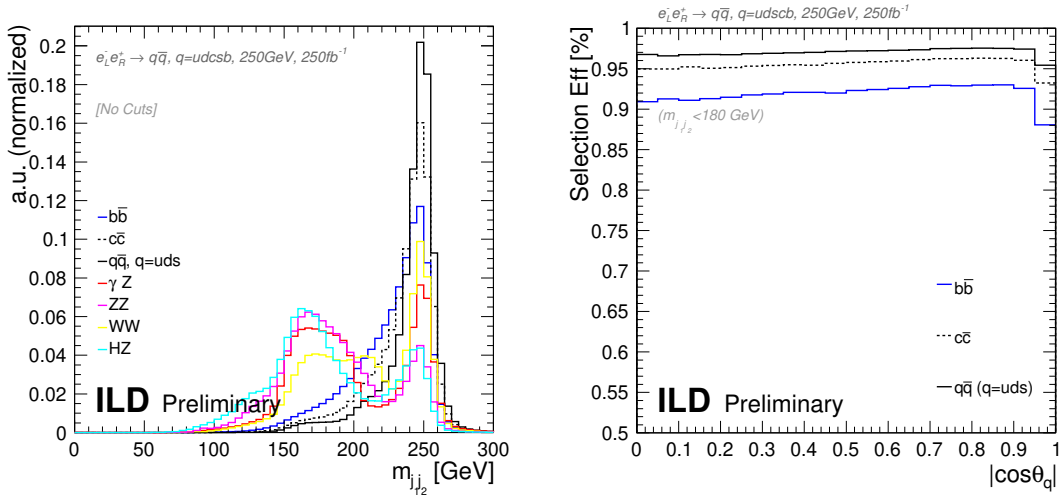


Figure 8: Invariant mass distribution

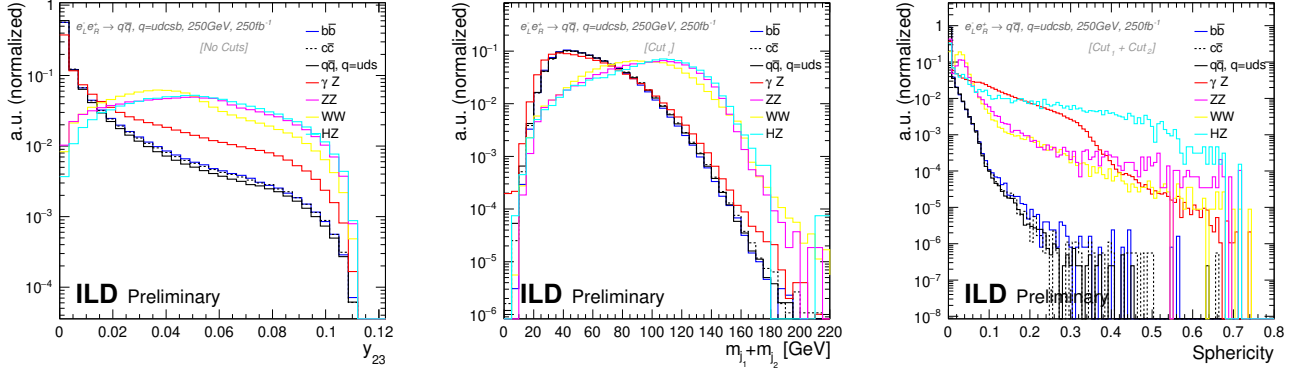


Figure 9: Topological variables used for the event preselection.

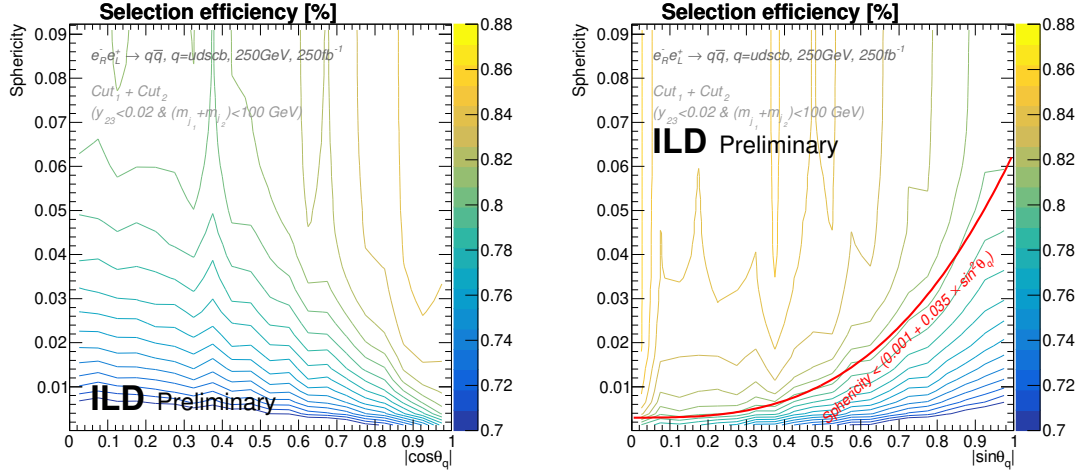


Figure 10: Efficiency of selection as a function of the θ angle and the sphericity.